CHAPTER FOUR

Dynamical properties of chaotic systems

In Chapter 3 we have concentrated on geometric aspects of chaos. In particular, we have discussed the fractal dimension characterization of strange attractors and their natural invariant measures, as well as issues concerning phase space dimensionality and embedding. In this chapter we concentrate on the time evolution dynamics of chaotic orbits. We begin with a discussion of the horseshoe map and symbolic dynamics.

4.1 The horseshoe map and symbolic dynamics

The horseshoe map was introduced by Smale (1967) as a motivating example in his development of *symbolic dynamics* as a basis for understanding a large class of dynamical systems. The horseshoe map $\mathbf{M}_h$ is specified geometrically in Figure 4.1. The map takes the square S (Figure 4.1(*a*)), uniformly stretches it vertically by a factor greater than 2 and uniformly compresses it horizontally by a factor less than $\frac{1}{2}$ (Figure 4.1(*b*)). Then the long thin strip is bent into a horseshoe shape with all the bending deformations taking place in the cross-hatched regions of Figures 4.1(*b*) and (*c*). Then the horseshoe is placed on top of the original square, as shown in Figure 4.1(*d*). Note that a certain fraction, which we denote $1 - f$, of the original area of the square S is mapped to the region outside the square. If initial conditions are spread over the square with a distribution which is uniform in the vertical direction, then the fraction of initial conditions that generate orbits that do not leave S during n applications of the map is just f^n. This is because a vertically uniform distribution in S remains vertically uniform on application of $\mathbf{M}_h$.

Since $f^n \to 0$ as $n \to \infty$, almost every initial condition with respect to Lebesgue measure eventually leaves the square. (Thus there is no attractor

contained in the square.[1]) We are interested in characterizing the invariant set Λ (which is of Lebesgue measure zero) of points which never leave the square. Furthermore, we wish to investigate the orbits followed by points in Λ. In order to do this, we first note that the intersection of the horseshoe with the square represents the regions that points in the square map to if they return to the square on one iterate. These regions are the

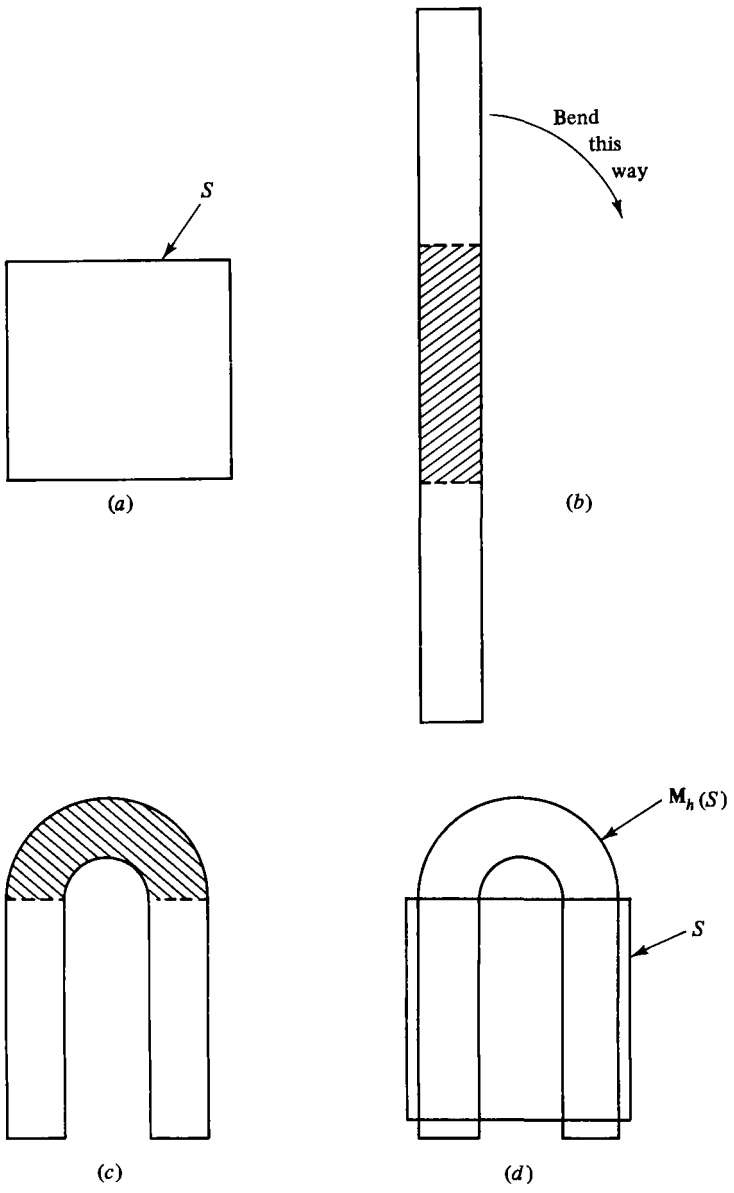

Figure 4 1 Construction of the horseshoe map.

two cross-hatched vertical strips labeled V_0 and V_1 in Figure 4.2(*a*). We now ask, where did these strips come from? To answer this question we follow the horseshoe construction in Figures 4.1(*a*)–(*d*) backward in time (i.e., from (*d*) to (*c*) to (*b*) to (*a*) in Figure 4.1). Thus, we find that the two vertical strips V_0 and V_1 are the images of two horizontal strips $H_0 = \mathbf{M}_h^{-1}(V_0)$ and $H_1 = \mathbf{M}_h^{-1}(V_1)$, as shown in Figure 4.2(*b*). Figure 4.2(*c*) shows what happens if we apply the horseshoe map to the vertical strips V_0 and V_1. Thus, taking the intersection of $\mathbf{M}_h(V_0)$ and $\mathbf{M}_h(V_1)$ with S (Figure 4.2(*d*)), we see that points originating in the square which remain in the square for two iterates of $\mathbf{M}_h$ are mapped to the four vertical strips labeled V_{00}, V_{01}, V_{10}, V_{11} in Figure 4.2(*d*). The subscripts on these strips V_{ij} are such that V_{ij} is contained in V_j and $\mathbf{M}_h^{-1}(V_{ij})$ is contained in V_i. Figure 4.2(*e*) shows the four horizontal strips that the vertical strips V_{ij} came from two iterates previous, $H_{ij} = \mathbf{M}_h^{-2}(V_{ij})$.

Now consider the invariant set Λ and the horizontal and vertical strips, H_0, H_1, V_0, V_1. Since points in Λ never leave S, the forward iterate of Λ must be in the square. Hence Λ is contained in $H_0 \cup H_1$ and is also

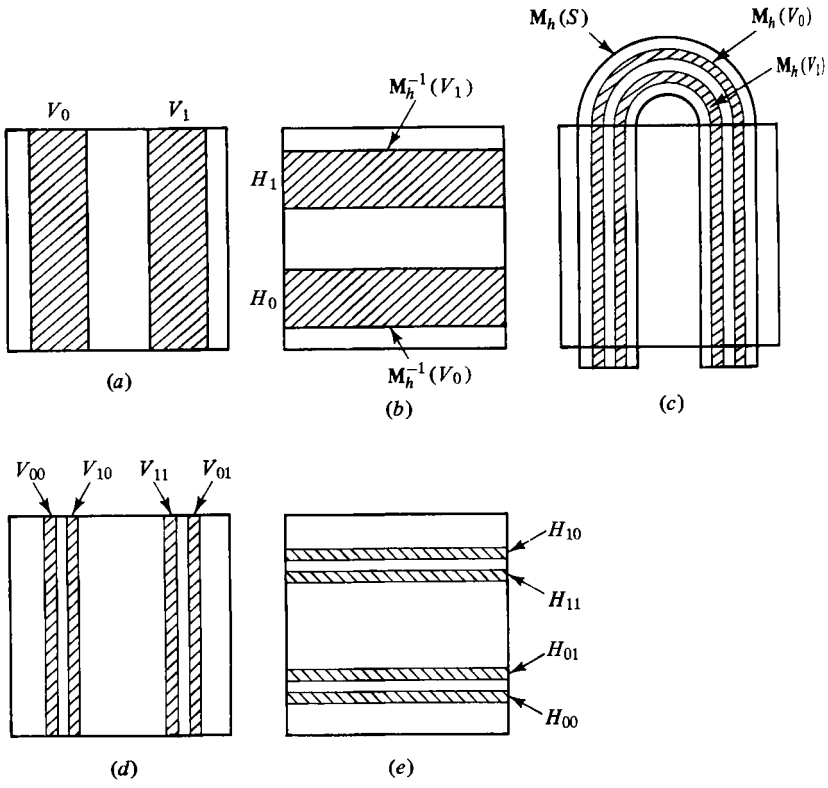

Figue 4.2 Vertical and horizontal strips V_i, V_{ij}, H_i and H_{ij} for the horseshoe map.

contained in $V_0 \cup V_1$. Thus, Λ is contained in the intersection,

$$(H_0 \cup H_1) \cap (V_0 \cup V_1).$$

This intersection consists of four squares as shown in Figure 4.3(*a*). Similarly Λ must also lie in the intersection

$$(H_{00} \cup H_{01} \cup H_{11} \cup H_{10}) \cap (V_{00} \cup V_{01} \cup V_{11} \cup V_{10})$$

shown in Figure 4.3(*b*). This intersection consists of 16 squares, four of which are contained in each of the four squares of Figure 4.3(*a*). Proceeding in stages of this type, at each successive stage, each square is replaced by four smaller squares that it contains. Taking the limit of repeating this construction an infinite number of times we obtain the invariant set Λ. This set is the intersection of a Cantor set of vertical lines (the Vs in the limit of an infinite number of iterations) with a Cantor set of horizontal lines (the Hs in the limit of an infinite number of iterations).

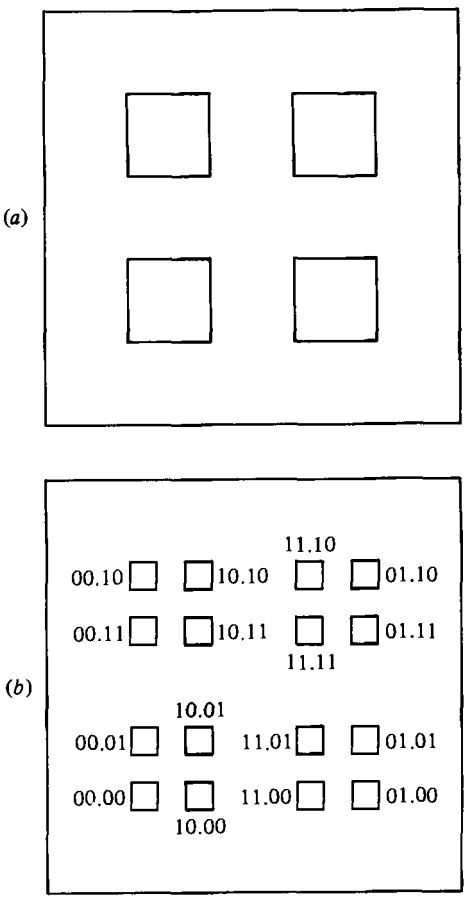

Figure 4.3(*a*) $(H_0 \cup H_1) \cap (V_0 \cup V_1)$ and (*b*) $(H_{00} \cup H_{01} \cup H_{11} \cup H_{10}) \cap (V_{00} \cup V_{01} \cup V_{10} \cup V_{11})$.

Let $\mathbf{x}$ be a point in the invariant set Λ. Then we claim that we can specify it by a bi-infinite symbol sequence $\mathbf{a}$,

$$\mathbf{a} = \ldots a_{-3}a_{-2}a_{-1} \cdot a_0 a_1 a_2 \ldots \tag{4.1}$$

and each symbol a_i is a function of $\mathbf{x}$ specified by

$$a_i = \begin{cases} 0 & \text{if } \mathbf{M}_h^i(\mathbf{x}) \text{ is in } H_0, \\ 1 & \text{if } \mathbf{M}_h^i(\mathbf{x}) \text{ is in } H_1. \end{cases} \tag{4.2}$$

The above represents a correspondence between bi-infinite symbol sequences $\mathbf{a}$ and points $\mathbf{x}$ in Λ. We denote this correspondence

$$\mathbf{a} = \phi(\mathbf{x}). \tag{4.3}$$

In Figure 4.3(*b*) we label the 16 rectangles by the symbols $a_{-2}a_{-1} \cdot a_0 a_1$ that correspond to the four middle symbols in (4.1) that all points in Λ that fall in that rectangle must have. The correspondence given by Eqs. (4.1)–(4.3) may be shown to be one to one and continuous (with a suitable definition of a metric on the space of bi-infinite symbol sequences). Define the *shift* operation,

$$\mathbf{a}' = \sigma(\mathbf{a}),$$

where $a_i' = a_{i+1}$. That is $\mathbf{a}'$ is obtained from $\mathbf{a}$ by moving the decimal point in Eq. (4.1) one place to the right. From Eq. (4.2) we have

$$a_i' = \begin{cases} 0 & \text{if } \mathbf{M}_h^{i+1}(\mathbf{x}) = \mathbf{M}_h^i(\mathbf{M}_h(\mathbf{x})) \text{ is in } H_0, \\ 1 & \text{if } \mathbf{M}_h^{i+1}(\mathbf{x}) = \mathbf{M}_h^i(\mathbf{M}_h(\mathbf{x})) \text{ is in } H_1. \end{cases}$$

Hence, $\mathbf{a}'$ is the symbol sequence corresponding to $\mathbf{M}_h(\mathbf{x})$, or $\sigma(\mathbf{a}) = \phi(\mathbf{M}_h(\mathbf{x}))$. We represent the situation schematically in Figure 4.4 Thus, the shift on the bi-infinite symbol space is equivalent to the horseshoe map applied to the invariant set Λ,

$$\mathbf{M}_{h|\Lambda} = \phi^{-1} \cdot \sigma \cdot \phi, \tag{4.4}$$

where $\mathbf{M}_{h|\Lambda}$ symbolizes the restriction of $\mathbf{M}_h$ to the invariant set Λ. Thus, to obtain $\mathbf{x}_{n+1}$ from $\mathbf{x}_n$ we can either apply $\mathbf{M}_h$ to $\mathbf{x}_n$, or else we can obtain $\mathbf{a}_n = \phi(\mathbf{x}_n)$, shift the decimal point to the right to get $\mathbf{a}_{n+1}$ and then obtain $\mathbf{x}_{n+1}$ from $\mathbf{x}_{n+1} = \phi^{-1}(\mathbf{a}_{n+1})$. Furthermore, to obtain $\mathbf{x}_{n+m}$ from $\mathbf{x}_n$ we

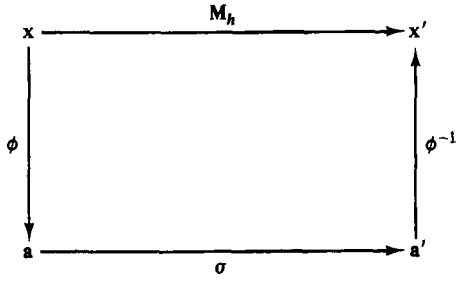

Figure 4.4 Equivalence of the shift operation σ and the horseshoe map.

can first get $\mathbf{a}_n = \phi(\mathbf{x}_n)$, then shift the decimal point m places to the right to get $\mathbf{a}_{n+m}$, and then obtain $\mathbf{x}_{n+m}$ from $\mathbf{x}_{n+m} = \phi^{-1}(\mathbf{a}_{n+m})$. For example, fixed points of σ^n are mapped by ϕ^{-1} to fixed points of $\mathbf{M}_h^n$. Since the former are just sequences that repeat after n shifts and since there are 2^n ways of choosing a sequence of n zeros and ones, we see that there are 2^n fixed points of $\mathbf{M}_h^n$ in Λ. This can be shown to imply that the set of points on periodic orbits is dense in the invariant set Λ. In addition, there is an uncountable set of nonperiodic orbits in Λ, and it may be shown that there are orbits which are dense in Λ. (If there is an orbit that is dense in an invariant set then we say that the set is *transitive*.) In Sections 2.1 and 3.1 we have established symbolic dynamics representations for one-dimensional noninvertible maps (Eqs. (2.3) and (3.3)) in which the system state was represented as an infinite sequence $(\cdot a_0 a_1 a_2 \ldots)$, as opposed to the bi-infinite sequence representation, Eq. (4.1). This difference comes about as a result of the noninvertibility of the maps of Sections 2.1 and 3.1. (This is reflected by the fact that the shift operating on $\cdot a_0 a_1 a_2 \ldots$ produces $\cdot a_1 a_2 a_3 \ldots$, and thus there is no information in the new symbol sequence of what a_0 is. Hence, we cannot go backward in time.) The correspondence we have established above between the horseshoe map and the shift of a bi-infinite symbol sequence of zeros and ones is an example of a reduction to symbolic dynamics that can be established for a large class of smooth invertible dynamical systems (in particular, systems having the property of hyperbolicity which we define later in this chapter).

As another example of symbolic dynamics, consider the map $\tilde{\mathbf{M}}$ geometrically shown in Figure 4.5(*a*). The map is similar to the horseshoe map, but contains an additional intersection with the square S, namely the region $\tilde{\mathbf{M}}(H_2)$. The three regions H_0, H_1 and H_2 shown in Figure 4.5(*b*) represent initial conditions that return to the square. We can again represent points $\mathbf{x}$ in the invariant set $\tilde{\Lambda}$ of the map $\tilde{\mathbf{M}}$ as points in a bi-infinite symbol sequence, Eq. (4.1), but now we need three symbols;

$$a_i = \begin{cases} 0 & \text{if } \tilde{\mathbf{M}}^i(\mathbf{x}) \text{ is in } H_0, \\ 1 & \text{if } \tilde{\mathbf{M}}^i(\mathbf{x}) \text{ is in } H_1, \\ 2 & \text{if } \tilde{\mathbf{M}}^i(\mathbf{x}) \text{ is in } H_2. \end{cases}$$

Again the operation of the map $\tilde{\mathbf{M}}$ corresponds to a shift σ operating on $\mathbf{a}$. There is, however, an important difference with the horseshoe. This is that all possible sequences of zeros, ones and twos are not allowed. In particular, we see from Figures 4.5(*a*) and (*b*) that points of $\tilde{\Lambda}$ that are in H_2 are always mapped by $\tilde{\mathbf{M}}$ to H_0 and not to H_1 or H_2 ($\tilde{\mathbf{M}}(H_2)$ intersects H_0 but does not intersect either H_1 or H_2). Thus, the possible allowable transitions are as shown in Figure 4.5(*c*). This means that whenever a 2 appears in our symbol sequence it is immediately followed by a zero (i.e.,

$a_i = 2$ implies $a_{i+1} = 0$). We call the symbolic dynamics corresponding to $\tilde{\mathbf{M}}$ a *shift of finite type* on three symbols (the phrase shift of finite type signifies a restriction on the allowed sequences), while we call the symbolic dynamics corresponding to the horseshoe map a *full shift* on two symbols (the word full signifying that there is no restriction on the allowed sequences).

As an application of symbolic dynamics, we mention the work of Levi (1981), who has analyzed a model periodically forced van der Pol equation (i.e., Eq. (1.13) with a periodic function of time on the right hand side). (Levi modifies the equation to facilitate his analysis.) Levi shows that the map obtained from the stroboscopic surface of section obtained by sampling at the forcing period (cf. Chapter 1) possesses an invariant set on which the dynamics is described by a shift of finite type on four symbols. Figure 4.5(*d*) shows the allowed transitions for Levi's problem

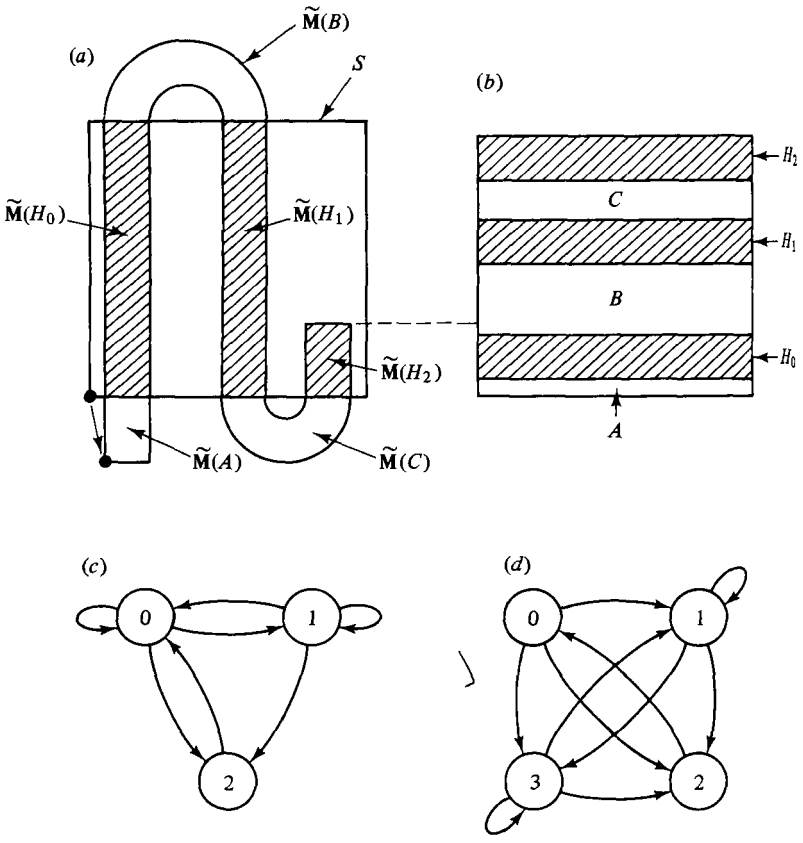

Figure 4.5(*a*) The map $\tilde{M}$. (*b*) $\tilde{M}(S) \cap S$ corresponds to the three strips H_0, H_1, H_2. (*c*) Allowed transitions for $\tilde{M}$; if x is in H_2 it is always in H_0 after one iterate. (*d*) Allowed transitions for Levi's problem.

4.2 Linear stability of steady states and periodic orbits

Consider a system of real first-order differential equations $\mathrm{d}\mathbf{x}/\mathrm{d}t = \mathbf{F}(\mathbf{x})$. A steady state for this system is a point $\mathbf{x} = \mathbf{x}_*$ at which

$$\mathbf{F}(\mathbf{x}_*) = 0.$$

We wish to examine the behaviour of orbits near $\mathbf{x}_*$. Thus we set

$$\mathbf{x}(t) = \mathbf{x}_* + \boldsymbol{\eta}(t),$$

where we assume $\boldsymbol{\eta}(t)$ is small. Substituting this into $\mathrm{d}\mathbf{x}/\mathrm{d}t = \mathbf{F}(\mathbf{x})$, we expand $\mathbf{F}(\mathbf{x})$ to first order $\boldsymbol{\eta}(t)$,

$$\mathbf{F}(\mathbf{x}_* + \boldsymbol{\eta}) = \mathbf{F}(\mathbf{x}_*) + \mathbf{DF}(\mathbf{x}_*)\cdot\boldsymbol{\eta} + O(\boldsymbol{\eta}^2),$$

where, since $\mathbf{x}_*$ is a steady state, $\mathbf{F}(\mathbf{x}_*) = 0$, and $\mathbf{DF}$ denotes the Jacobian matrix of partial derivatives of $\mathbf{F}$. That is, if we write

$$\mathbf{x} = \begin{bmatrix} x^{(1)} \\ x^{(2)} \\ \vdots \\ x^{(N)} \end{bmatrix}, \quad \mathbf{F}(\mathbf{x}) = \begin{bmatrix} F^{(1)}(x^{(1)}, x^{(2)}, \ldots, x^{(N)}) \\ F^{(2)}(x^{(1)}, x^{(2)}, \ldots, x^{(N)}) \\ \vdots \\ F^{N}(x^{(1)}, x^{(2)}, \ldots, x^{(N)}) \end{bmatrix},$$

then

$$\mathbf{DF}(\mathbf{x}) = \begin{bmatrix} \partial F^{(1)}/\partial x^{(1)} & \partial F^{(1)}/\partial x^{(2)} & \ldots & \partial F^{(1)}/\partial x^{(N)} \\ \partial F^{(2)}/\partial x^{(1)} & \partial F^{(2)}/\partial x^{(2)} & \ldots & \partial F^{(2)}/\partial x^{(N)} \\ \vdots & \vdots & & \vdots \\ \partial F^{(N)}/\partial x^{(1)} & \partial F^{(N)}/\partial x^{(2)} & \ldots & \partial F^{(N)}/\partial x^{(N)} \end{bmatrix}$$

We obtain the following equation for the time dependence of the perturbation of $\mathbf{x}$ from the steady state

$$\mathrm{d}\boldsymbol{\eta}/\mathrm{d}t = \mathbf{DF}(\mathbf{x}_*)\cdot\boldsymbol{\eta} + O(\boldsymbol{\eta}^2). \tag{4.5}$$

The linearized stability problem is obtained by neglecting terms of order $\boldsymbol{\eta}^2$ in (4.5) and is of the general form

$$\mathrm{d}\mathbf{y}/\mathrm{d}t = \mathbf{A}\cdot\mathbf{y}, \tag{4.6}$$

where $\mathbf{y}$ is a real N-dimensional vector and $\mathbf{A}$ is a real time-independent $N \times N$ matrix. If we seek solutions of Eq. (4.6) of the form $\mathbf{y}(t) = \mathbf{e}\exp(st)$, then (4.6) becomes the eigenvalue equation

$$\mathbf{A}\cdot\mathbf{e} = s\mathbf{e}, \tag{4.7}$$

which has nontrivial solutions for values of s satisfying the Nth order polynomial equation

$$D(s) = \det[\mathbf{A} - s\mathbf{I}] = 0, \tag{4.8}$$

where $\mathbf{I}$ denotes the $N \times N$ identity matrix. For our purposes it suffices to consider only the case where $D(s) = 0$ has N *distinct* roots $s = s_k$ for

$k = 1, 2, \ldots, N$, (i.e., $s_k \neq s_j$ if $k \neq j$). For each such root there is an eigenvector $\mathbf{e}_k$, and any time evolution can be represented as

$$\mathbf{y}(t) = \sum_{k=1}^{N} A_k \mathbf{e}_k \exp(s_k t), \tag{4.9}$$

where the A_k are constant coefficients (that may be complex) determined from the initial condition $\mathbf{y}(0) = \Sigma_{i=1}^{N} A_k \mathbf{e}_k$. Since the coefficients of the polynomial $D(s)$ are real, the eigenvalues s_k are either real or else occur in complex conjugate pairs.

In the case of complex conjugate pairs of eigenvalues $s_j = s_{j+1}^* = \sigma_j - i\omega_j$, we can also take $\mathbf{e}_j = \mathbf{e}_{j+1}^* = \mathbf{e}_j^R + i\mathbf{e}_j^I$, where the * denotes complex conjugate, and σ_j, ω_j, $\mathbf{e}_j^R$ and $\mathbf{e}_j^I$ are all real. Combining the two solutions, j and $j+1$, we obtain two linearly independent *real* solutions,

$$\begin{aligned}\mathbf{g}_j(t) &= \tfrac{1}{2}[\mathbf{e}_j \exp(s_j t) + \mathbf{e}_{j+1} \exp(s_{j+1} t)] \\ &= \mathbf{e}_j^R \exp(\sigma_j t)\cos(\omega_j t) + \mathbf{e}_j^I \exp(\sigma_j t)\sin(\omega_j t), \end{aligned} \tag{4.10a}$$

$$\begin{aligned}\mathbf{g}_{j+1}(t) &= \frac{1}{2i}[\mathbf{e}_j \exp(s_j t) - \mathbf{e}_{j+1} \exp(s_{j+1} t)] \\ &= \mathbf{e}_j^I \exp(\sigma_j t)\sin(\omega_j t) - \mathbf{e}_j^R \exp(\sigma_j t)\cos(\omega_j t). \end{aligned} \tag{4.10b}$$

If s_j is real ($s_j = \sigma_j$), then we write $\mathbf{g}_j(t) = \mathbf{e}_j \exp(\sigma_j t)$ (where $\mathbf{e}_j$ is real). Equation (4.9) thus becomes

$$\mathbf{y}(t) = \sum_{j=1}^{N} B_j \mathbf{g}_j(t), \tag{4.11}$$

where (in contrast with the coefficients A_k of Eq. (4.9)) all the B_j are *real*. By use of a similarity transformation

$$\mathbf{z}(t) = \mathbf{T} \cdot \mathbf{y}(t), \tag{4.12}$$

where $\mathbf{T}$ is a real $N \times N$ matrix, we can recast Eq. (4.6) as

$$d\mathbf{z}/dt = \mathbf{C} \cdot \mathbf{z}, \quad \mathbf{C} = \mathbf{T} \cdot \mathbf{A} \cdot \mathbf{T}^{-1}. \tag{4.13}$$

where, if there are K real eigenvalues, $\sigma_1, \sigma_2, \ldots, \sigma_k$, and $N - K$ complex conjugate eigenvalues, then the real $N \times N$ matrix $\mathbf{C}$ has the following *canonical form*,

$$\mathbf{C} = \begin{bmatrix} \mathbf{\Sigma} & \mathbf{O} \\ \mathbf{O} & \mathbf{\Lambda} \end{bmatrix}, \tag{4.14}$$

where $\mathbf{\Sigma}$ is a $K \times K$ diagonal matrix

$$\mathbf{\Sigma} = \begin{bmatrix} \sigma_1 & 0 & 0 & \ldots & 0 \\ 0 & \sigma_2 & 0 & \ldots & 0 \\ 0 & 0 & \sigma_3 & \ldots & 0 \\ \vdots & \vdots & \vdots & & \vdots \\ 0 & 0 & 0 & \ldots & \sigma_K \end{bmatrix}, \tag{4.15}$$

and Λ is a real matrix of 2×2 blocks along its diagonal

$$\Lambda = \begin{bmatrix} \Lambda_1 & \mathbf{O} & \mathbf{O} & \cdots \\ \mathbf{O} & \Lambda_2 & \mathbf{O} & \cdots \\ \mathbf{O} & \mathbf{O} & \Lambda_3 & \cdots \\ \vdots & \vdots & \vdots & \end{bmatrix} \tag{4.16}$$

with the 2×2 matrix block Λ_m having the form

$$\Lambda_m = \begin{bmatrix} \sigma_m & \omega_m \\ -\omega_m & \sigma_m \end{bmatrix}, \tag{4.17}$$

and $\mathbf{O}$ being 2×2 matrices of zeros.

For $\mathrm{Re}(s_j) = \sigma_j < 0$, the corresponding solution $\mathbf{g}_j(t)$ approaches the origin asymptotically in time, either spiraling in the plane spanned by $\mathbf{e}_j^R$ and $\mathbf{e}_j^I$ if $\mathrm{Im}(s_j) \neq 0$, or else by moving along the line through the origin in the direction of the real eigenvector $\mathbf{e}_j$ if $\mathrm{Im}(s_j) = 0$. For $\mathrm{Re}(s_j) = \sigma_j > 0$, the corresponding solution $\mathbf{g}_j(t)$ diverges from the origin exponentially in time, either (as for $\sigma_j < 0$) by spiraling or by moving linearly. We call solutions which move away from the origin exponentially with time *unstable* and those that move exponentially toward the origin *stable*. The situation is as illustrated in Figure 4.6.

Note that for the case $\omega_j \neq 0$ any initial condition purely in the subspace spanned by the vectors $\mathbf{e}_j^R$ and $\mathbf{e}_j^I$ remains in that subspace for all time. Hence, that subspace is invariant under the flow $d\mathbf{y}/dt = \mathbf{A} \cdot \mathbf{y}$. Similarly, if the eigenvalue is real ($s_j = \sigma_j$), then an initial condition on the ray from the origin along $\mathbf{e}_j$ remains on that ray, and hence the set of

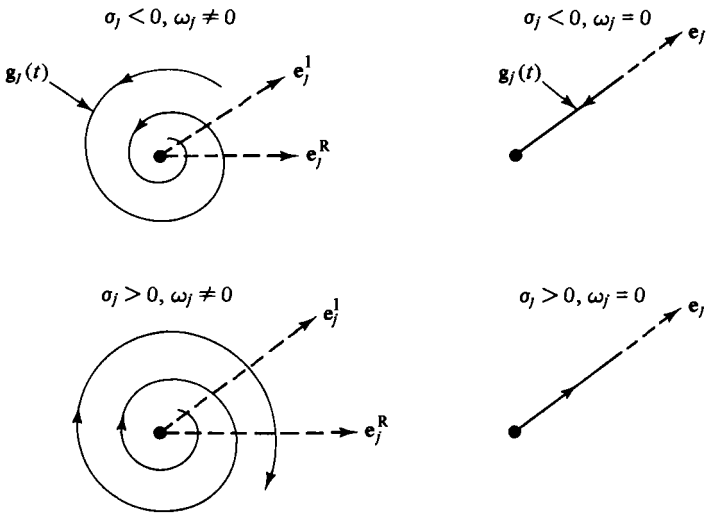

Figure 4.6 Stable ($\sigma_j < 0$) and unstable ($\sigma_j > 0$) orbits.

vectors that are scalar multiples of $\mathbf{e}_j$ is an invariant subspace. We collect all the independent vectors spanning invariant subspaces corresponding to unstable solutions ($\sigma_j > 0$) and denote them

$$\mathbf{u}_1, \mathbf{u}_2, \ldots, \mathbf{u}_{n_u}.$$

Similarly, we collect all the independent vectors spanning invariant subspaces corresponding to stable solutions ($\sigma_j < 0$) and denote them

$$\mathbf{v}_1, \mathbf{v}_2, \ldots, \mathbf{v}_{n_s}$$

If there are eigenvalues whose real parts are zero ($\sigma_j = 0$), we denote the corresponding set of independent vectors spanning this subspace

$$\mathbf{w}_1, \mathbf{w}_2, \ldots, \mathbf{w}_{n_c}$$

All of the us, vs and ws, taken together, span the whole phase space. Thus

$$n_u + n_s + n_c = N.$$

We define the *unstable subspace* as

$$E^u = \text{span}[\mathbf{u}_1, \mathbf{u}_2, \ldots, \mathbf{u}_{n_u}],$$

(i.e., the space spanned by the vector $\mathbf{u}_1, \mathbf{u}_2, \mathbf{u}_3, \ldots, \mathbf{u}_{n_u}$) the *stable subspace* as

$$E^s = \text{span}[\mathbf{v}_1, \mathbf{v}_2, \ldots, \mathbf{v}_{n_s}],$$

and the *center subspace* as

$$E^c = \text{span}[\mathbf{w}_1, \mathbf{w}_2, \ldots, \mathbf{w}_{n_c}].$$

Figure 4.7 illustrates some cases of stable and unstable subspaces and the corresponding orbits ($n_c = 0$ in Figure 4.7: (*a*) $N = 2$, $n_u = n_s = 1$, (*b*) $N = 3$, $n_u = 1$ and $n_s = 2$, where the stable space corresponds to two real eigenvalues; (*c*) $N = 3$, $n_u = 1$ and $n_s = 2$, where the stable subspace corresponds to a pair of complex conjugate eigenvalues; and (*d*) $N = 3$, $n_s = 1$ and $n_u = 2$, where the unstable subspace corresponds to a pair of complex conjugate eigenvalues).

We now turn from the study of the linear stability of a steady state $\mathbf{x} = \mathbf{x}_*$, to the study of the stability of a periodic orbit,

$$\mathbf{x}(t) = \mathbf{X}_*(t) = \mathbf{X}_*(t + T),$$

where T denotes the period. As for the case of the steady state, we write

$$\mathbf{x}(t) = \mathbf{X}_*(t) + \boldsymbol{\eta}(t)$$

and expand for small $\boldsymbol{\eta}(t)$. We obtain

$$d\boldsymbol{\eta}/dt = \mathbf{DF}(\mathbf{X}_*(t)) \cdot \boldsymbol{\eta} + O(\boldsymbol{\eta}^2), \tag{4.18}$$

which is similar to (4.5) except that now the matrix $\mathbf{DF}(\mathbf{X}_*(t))$ varies periodically in time, whereas $\mathbf{DF}(\mathbf{x}_*)$ in (4.5) is independent of time. The linearized stability problem is of the form

$$d\mathbf{y}/dt = \mathbf{A}(t) \cdot \mathbf{y}, \tag{4.19}$$

where $\mathbf{y}$ is a real N-dimensional vector and $\mathbf{A}(t)$ is a real time periodic $N \times N$ matrix,

$$\mathbf{A}(t) = \mathbf{A}(t + T).$$

Solutions of (4.19) can be sought in the Floquet form,

$$\mathbf{e}(t)\exp(st),$$

where $\mathbf{e}(t)$ is periodic in time $\mathbf{e}(t) = \mathbf{e}(t + T)$. This defines an eigenvalue problem for eigenvalues s_j and vector eigenfunctions $\mathbf{e}_j(t)$. A development parallel to that for Eq. (4.6) goes through, and stable, unstable, and center subspaces can be analogously defined, although the solution of the Floquet problem is much more difficult. One result for the system (4.18) is immediate, however. Namely, Eq. (4.18) has a solution corresponding to a zero eigenvalue ($s = 0$). To see this, differentiate the equation $d\mathbf{X}_*(t)/dt = \mathbf{F}(\mathbf{X}_*(t))$ with respect to time. This gives an equation of the form of Eq. (4.19), $d\mathbf{e}_0(t)/dt = \mathbf{DF}(\mathbf{X}_*(t)) \cdot \mathbf{e}_0(t)$, where $\mathbf{e}_0(t) \equiv d\mathbf{X}_*(t)/dt$. This zero eigenvalue solution can be interpreted as saying that, if the perturbation $\eta(t)$ puts the perturbed orbit on the closed phase space curve

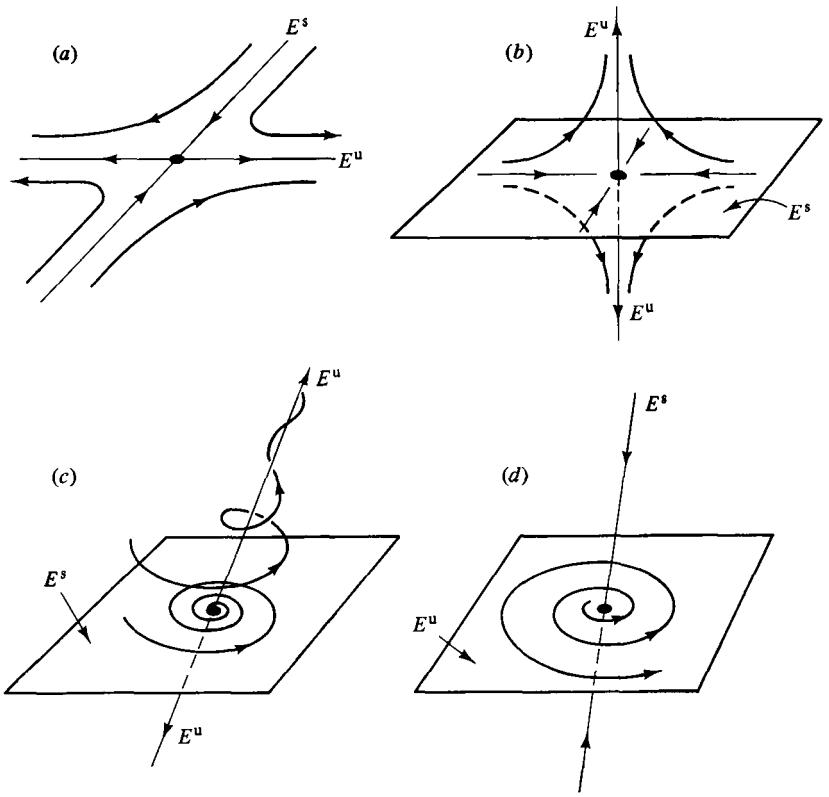

Figure 4.7 Stable and unstable subspaces.

followed by $\mathbf{X}_*(t)$ but slightly displaced from $\mathbf{X}_*(t)$, then $\eta(t)$ varies periodically in time ($s = 0$). This is illustrated in Figure 4.8(*a*).

Instead of pursuing the Floquet solutions further, we employ a surface of section to reduce the problem $d\mathbf{x}/dt = \mathbf{F}(\mathbf{x})$ to a map $\hat{\mathbf{x}}_{n+1} = \mathbf{M}(\hat{\mathbf{x}}_n)$, where $\hat{\mathbf{x}}_n$ has lower dimensionality than $\mathbf{x}$ by one. As shown in Figure 4.8(*b*), we assume that the periodic solution $\mathbf{X}_*(t)$ results in a fixed point $\hat{\mathbf{x}}_*$ of the map. Linearizing the map around $\hat{\mathbf{x}}_*$ by writing $\hat{\mathbf{x}}_n = \hat{\mathbf{x}}_* + \hat{\boldsymbol{\eta}}_n$ with $\hat{\boldsymbol{\eta}}_n$ small, we obtain

$$\hat{\boldsymbol{\eta}}_n = \mathbf{DM}(\hat{\mathbf{x}}_*) \cdot \hat{\boldsymbol{\eta}}_n + O(\hat{\boldsymbol{\eta}}_n^2), \tag{4.20}$$

which yields a linearized problem of the form

$$\hat{\mathbf{y}}_{n+1} = \hat{\mathbf{A}} \cdot \mathbf{y}_n. \tag{4.21}$$

Seeking solutions $\hat{\mathbf{y}} = \lambda^n \hat{\mathbf{e}}$, we obtain the eigenvalue equation

$$\hat{\mathbf{A}} \cdot \hat{\mathbf{e}} = \lambda \hat{\mathbf{e}}. \tag{4.22}$$

Again we assume eigenvalue solutions λ_j of the determinantal equation,

$$\hat{D}(\lambda) = \det[\hat{\mathbf{A}} - \lambda \mathbf{I}] = 0, \tag{4.23}$$

and denote the corresponding eigenvectors $\hat{\mathbf{e}}_j$. Directions corresponding to $|\lambda_j| > 1$ are unstable; directions corresponding to $|\lambda_j| < 1$ are stable. Again, we can identify unstable, stable and center subspaces, E^u, E^s and E^c, for the map (e.g., the stable subspace is spanned by the real and imaginary parts of all those vectors $\hat{\mathbf{e}}_j$ for which $|\lambda_j| < 1$).

The map eigenvalues and the Floquet eigenvalues are related by

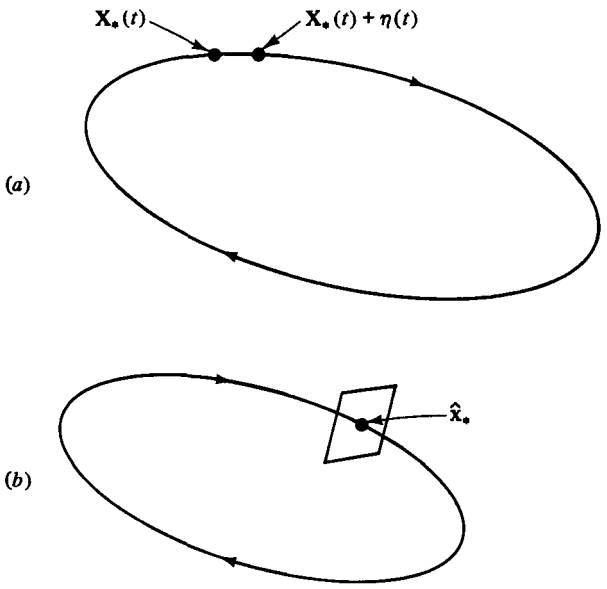

Figure 4.8(*a*) The zero eigenvalue solution of (4.18). (*b*) Surface of section for a periodic orbit.

$$\lambda_j = \exp(s_j T), \tag{4.24}$$

and all the s_j of the Floquet problem are included except for the zero eigenvalue illustrated in Figure 4.8(*a*). The zero eigenvalue is not included because a perturbation $\boldsymbol{\eta}$ that displaces the orbit along the closed curve path followed by $\mathbf{X}_*(t)$ results in no perturbation of the orbit's surface of section piercing at $\hat{\mathbf{x}} = \hat{\mathbf{x}}_*$ (cf. Figure 4.8).

We remark that we have assumed in the above that the periodic orbit results in a fixed point of the surface of section map. If instead it results in a period p orbit (as shown in Figure 4.9 for $p = 3$), $\hat{\mathbf{x}}_0^* \to \hat{\mathbf{x}}_1^* \to \cdots \to \hat{\mathbf{x}}_p^* = \hat{\mathbf{x}}_0^*$, then we select one of the p points $\hat{\mathbf{x}}_j^*$ on the map orbit and examine the pth iterate of the map $\mathbf{M}^p$. For the map $\mathbf{M}^p$ the point $\hat{\mathbf{x}}_p^*$ is a fixed point,

$$\hat{\mathbf{x}}_j^* = \mathbf{M}^p(\hat{\mathbf{x}}_j^*). \tag{4.25}$$

Linearizing about this point, we again have a problem of the form of (4.21), but now $\mathbf{A}$ is identified with $\mathbf{DM}^p(\hat{\mathbf{x}}_j^*)$. We note that the chain rule for differentiation yields

$$\mathbf{DM}^p(\hat{\mathbf{x}}_j^*) = \mathbf{DM}(\hat{\mathbf{x}}_{j-1}^*)\mathbf{DM}(\hat{\mathbf{x}}_{j-1}^*)\ldots\mathbf{DM}(\hat{\mathbf{x}}_0^*)\mathbf{DM}(\hat{\mathbf{x}}_{p-1}^*)\ldots\mathbf{DM}(\hat{\mathbf{x}}_j^*). \tag{4.26}$$

This is a matrix version of the one-dimensional map result Eq. (2.7). Finally, we wish to stress that, although we have been discussing the map $\mathbf{M}$ as arising from a surface of section of a continuous time system, our discussion connected with Eqs. (4.20)–(4.23) and (4.25)–(4.26) applies to maps in general, whether they arise via a surface of section or not. (As an example of the latter, Problem 5 deals with the stability of a periodic orbit of the Hénon map.)

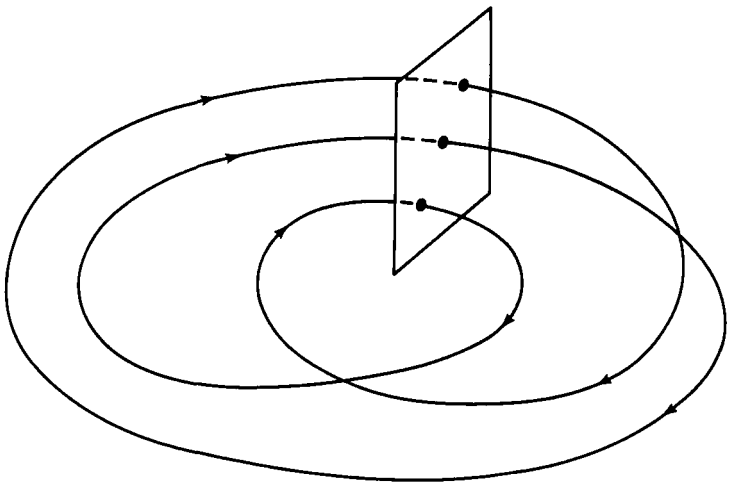

Figue 4.9 Period three orbit of the surface of section map $\mathbf{M}$.

4.3 Stable and unstable manifolds

We define stable and unstable manifolds of steady states and periodic orbits of smooth dynamical systems as follows. The *stable manifold* of a steady state or periodic orbit is the set of points $\mathbf{x}$ such that the forward orbit starting from $\mathbf{x}$ approaches the steady state or the closed curve traced out by the periodic orbit. Similarly, the *unstable manifold* of a steady state or periodic orbit is the set of points $\mathbf{x}$ such that the orbit going backward in time starting from $\mathbf{x}$ approaches the steady state or the closed curve traced out by the periodic orbit (this assumes invertibility if we are dealing with a map). The existence and smoothness of these manifolds can be proven under very general conditions. Furthermore, stable and unstable manifolds, W^s and W^u, of a steady state or periodic orbit, have the same dimensionality as the linear subspace E^s and E^u and are tangent to them,

$$\dim(W^s) = n_s,$$
$$\dim(W^u) = n_u.$$

Figure 4.10 (*a*) illustrates the situation for a two-dimensional map with a fixed point γ that has one stable and one unstable direction. Figure 4.10(*b*) applies for a situation where $n_s = 2$ and $n_u = 1$ for a fixed point γ of a flow Also, in Figure 4.10(*b*), we show an orbit in $W^s(\gamma)$ spiraling into the fixed point γ for the case where the two stable eigenvalues are complex conjugates.

For specificity, in what follows we will only be considering the case of periodic orbits of an invertible map where the orbit period is 1 (i.e., fixed points of the map). We now show that stable manifolds cannot intersect stable manifolds, and unstable manifolds cannot intersect unstable manifolds. For the case of self-intersections of an unstable manifold, this follows from the following considerations. Very near the fixed point γ, say within a distance ε, the unstable manifold is a small section of an n_u-dimensional surface tangent to E^u. Call this small piece of the unstable manifold $W^u_\varepsilon(\gamma)$. Since $W^u_\varepsilon(\gamma)$ lies close to the n_u-dimensional plane E^u, it does not intersect itself. Now, continually mapping the small surface $W^u_\varepsilon(\gamma)$ forward in time, it expands in all its n_u unstable directions filling out the whole unstable manifold of γ, $W^u(\gamma)$. Since we assume the map is invertible, two distinct points cannot be mapped to the same point. Thus, $W^u(\gamma)$ cannot intersect itself. Now consider two distinct fixed points γ_1 and γ_2 with unstable manifolds $W^u(\gamma_1)$ and $W^u(\gamma_2)$. These cannot intersect each other because, if they did, then a backward orbit starting at an intersection point would have to approach both γ_1 and γ_2 in the limit of an infinite number of backwards iterates. However, $\gamma_1 \neq \gamma_2$; so this is

impossible. Hence there can be no intersections of unstable manifolds, and, applying a similar argument, with the direction of time reversed, there can be no intersection of stable manifolds.

We note, however, that stable and unstable manifolds can intersect each other. In Figure 4.10(*c*) we show an intersection of stable and unstable manifolds of a fixed point γ of a two-dimensional map. This is

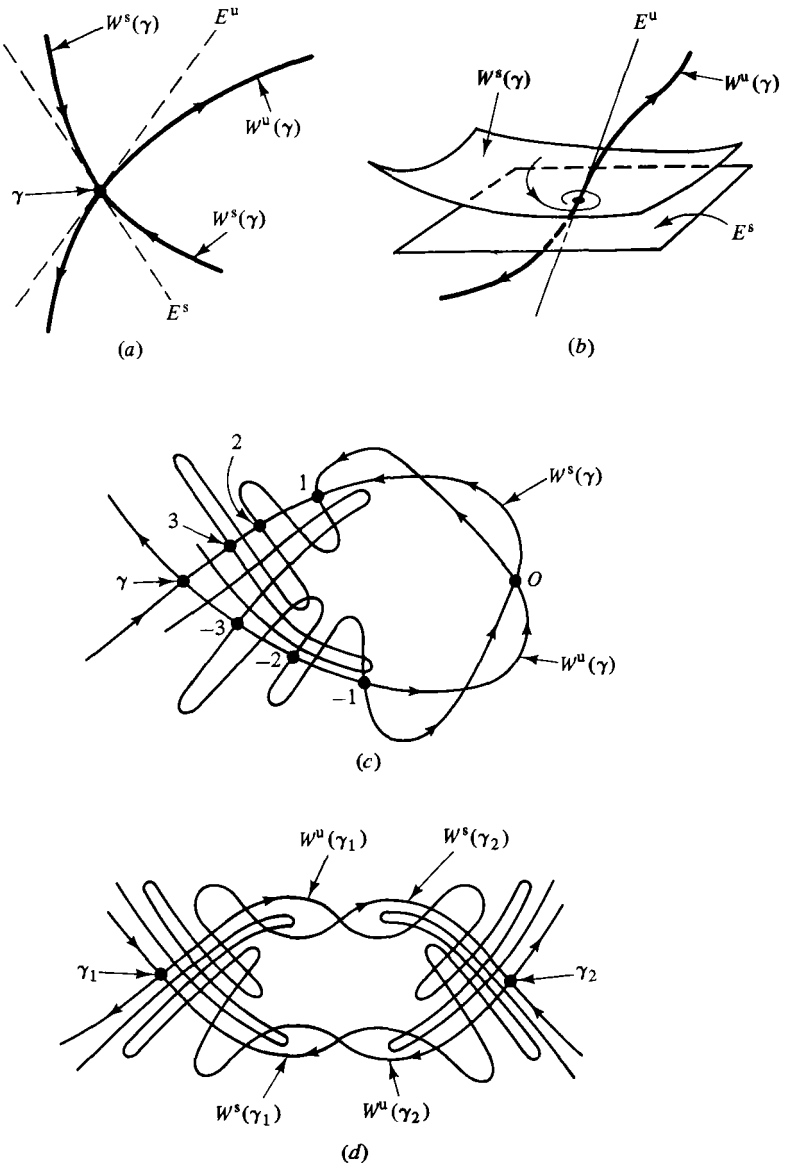

Figure 4.10 Stable and unstable manifolds.

called a *homoclinic intersection.* In Figure 4.10(*d*) we show intersections of the stable and unstable manifolds of one fixed point γ_1 with those of another fixed point γ_2. This is called a *heteroclinic intersection.* The complexity of these diagrams stems from the fact that, if a stable and unstable manifold intersect once, then they must intersect an infinite number of times. To see this, we have labeled one of the intersections O in Figure 4.10(*c*). Since O is on $W^s(\gamma)$ and $W^u(\gamma)$ its subsequent iterates, both forward and backward in time, must also be on $W^s(\gamma)$ and $W^u(\gamma)$, because $W^s(\gamma)$ and $W^u(\gamma)$ are invariant sets by their construction. Thus intersection points map into intersection points. Iterating the point O forward in time, it approaches γ along the stable manifold, successively mapping to the points labeled 1, 2 and 3 in Figure 4.10(*c*). Iterating the point 0 backward in time, it approaches γ along the unstable manifold, successively mapping to the points labeled -1, -2 and -3. The complicated nature of Figures 4.10(*c*) and (*d*) suggests complicated dynamics when homoclinic or heteroclinic intersections are present. Indeed this is so Smale (1967) shows that a homoclinic intersection implies horseshoe type dynamics for some sufficiently high iterate of the map. To see this consider the homoclinic intersection for the fixed point γ shown in Figure 4.11(*a*). The manifolds $W^s(\gamma)$ and $W^u(\gamma)$ intersect at the point ξ. Choosing a small rectangle J about the point γ and mapping it forward in time a sufficient number of iterates q_+ we obtain $\mathbf{M}^{q_+}(J)$. Similarly mapping J backward q_- iterates, we obtain the region $\mathbf{M}^{-q_-}(J) \equiv S$. (See Figure 4.11(*b*)). Thus we have the picture shown in Figure 4.11(*c*) which shows that $\mathbf{M}^q$, where $q = q_+ + q_-$, maps S to a horseshoe as in Figure 4.1. Hence, $\mathbf{M}^q$ is a horseshoe map on the long thin rectangle S and has an invariant set in S on which the dynamics is equivalent to a full shift on two symbols. We note that, although we have drawn the shapes of $W^s(\gamma)$ and $W^u(\gamma)$ in Figure 4.11(*a*) to make the horseshoe shape obvious (Figure 4.11(*c*)), the result stated above and proved by Smale depends only on the existence of a homoclinic intersection.[2] Furthermore, a similar result applies in the heteroclinic case, Figure 4.10(*d*).

In Section 4.2 we have discussed the linearized map $\mathbf{y}_{n+1} = \mathbf{A} \cdot \mathbf{y}_n$ about a fixed point $\mathbf{x}_*$, and the splitting of the vector space in which $\mathbf{y}$ lies into subspaces E^s, E^u and E^c that are invariant under the matrix $\mathbf{A}$. We call the vectors $\mathbf{y}$ *tangent vectors.* We call the space in which they lie the *tangent space* of the map at $\mathbf{x} = \mathbf{x}_*$, and we denote this space $T_{\mathbf{x}_*}$.

We say the fixed point $\mathbf{x}_*$ is *hyperbolic* if there is no center subspace E^c That is, if all the magnitudes of the eigenvalues λ_j are either greater than 1 or less than 1, and $n_u + n_s$ is the dimension of $\mathbf{y}$. In this case, we say that the tangent space $T_{\mathbf{x}_*}$ has a direct sum decomposition into E^s and E^u, $T_{\mathbf{x}_*} = E^s \oplus E^u$. That is, vectors in the space $T_{\mathbf{x}_*}$ can be uniquely specified

as the sum of two component vectors, one in the subspace E^s and one in the subspace E^u.

There is a notion of hyperbolicity not only for fixed points, but also for more general invariant sets of a map. Such an invariant set might be, for example, a strange attractor (the strange attractor of the generalized baker's map is hyperbolic), or it may not be an attractor (like the invariant set of the horseshoe map).

We say that an invariant set Σ is *hyperbolic* if there is a direct sum decomposition of T_x into stable and unstable subspace $T_x = E_x^s \oplus E_x^u$ for

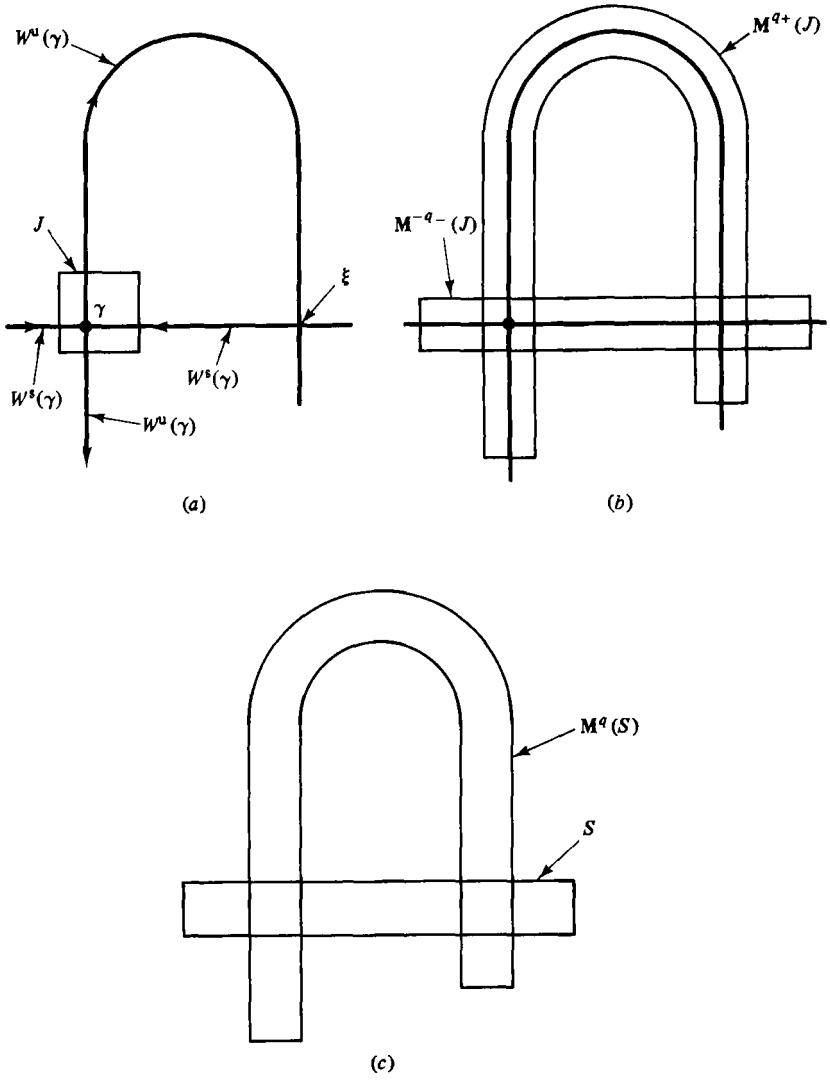

Figure 4.11 Construction of a horseshoe from a homoclinic intersection.

all $\mathbf{x}$ in Σ, such that the splitting into $E^s_{\mathbf{x}}$ and $E^u_{\mathbf{x}}$ varies continuously with $\mathbf{x}$ in Σ and is invariant in the sense that $\mathbf{DM}(E^{s,u}_{\mathbf{x}}) = E^{s,u}_{\mathbf{M}(\mathbf{x})}$, and there are some numbers $K > 0$ and $0 < \rho < 1$ such that the following hold.

(*a*) If $\mathbf{y}$ is in $E^s_{\mathbf{x}}$ then

$$|\mathbf{DM}^n(\mathbf{x}) \cdot \mathbf{y}| < K\rho^n|\mathbf{y}|. \tag{4.27a}$$

(*b*) If $\mathbf{y}$ is in $E^u_{\mathbf{x}}$ then

$$|\mathbf{DM}^{-n}(\mathbf{x}) \cdot \mathbf{y}| < K\rho^n|\mathbf{y}|. \tag{4.27b}$$

Consider $\mathbf{x}$ as an initial condition. Conditions (*a*) and (*b*) basically say that the orbit originating from another initial condition infinitesimally displaced from $\mathbf{x}$ exponentially approaches the orbit, $\mathbf{M}^n(\mathbf{x})$ or exponentially diverges from it if the infinitesimal displacement is in $E^s_{\mathbf{x}}$ or $E^u_{\mathbf{x}}$, respectively.

Hyperbolic invariant sets are mainly of interest because the property of hyperbolicity allows many interesting mathematically rigorous results to be obtained. Much of what is rigorously known about the structure and dynamics of chaos is only known for cases which satisfy the hyperbolicity conditions. (See, for example, the text by Guckenheimer and Holmes (1983).) Some of these results are the following (some restrictions in addition to hyperbolicity are also required for some of these statements)

(1) Stable and unstable manifolds at $\mathbf{x}$ in Σ, denoted $W^s(\mathbf{x})$ and $W^u(\mathbf{x})$, can be locally defined. Two points on the same stable manifold, for example, approach each other exponentially in time as illustrated in Figure 4.12. Note that $W^{s,u}(\mathbf{x})$ is tangent to $E^{s,u}_{\mathbf{x}}$ at $\mathbf{x}$.

(2) If small noise is added to a hyperbolic system with a chaotic attractor, then a resulting noisy orbit perturbed from the chaotic attractor can be 'shadowed' by a 'true' orbit of the noiseless system such that the

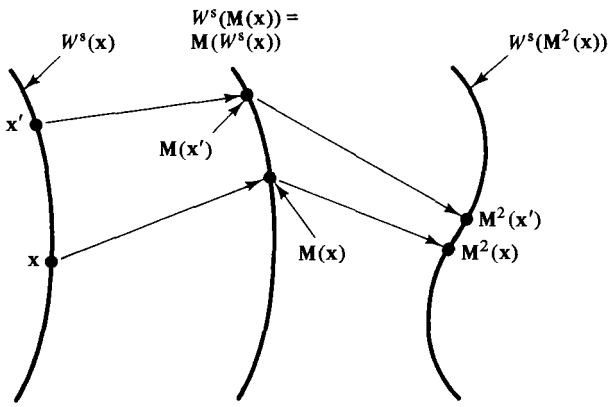

Figure 4.12 Illustration of the stable manifold.

true orbit closely follows the noisy orbit (see Section 1.5 and Problem 2 of Chapter 2 for other discussions of shadowing).

(3) The dynamics on the invariant set can be represented via symbolic dynamics as a full shift or a shift of finite type on a bi-infinite symbol sequence (as illustrated in Figure 4.4).

(4) If the invariant hyperbolic set is an attractor, then a natural measure (as defined in Chapter 2) exists.

(5) The invariant set and its dynamics are *structurally stable* in the sense that small smooth perturbations of the map preserve the dynamics. In particular, if $\mathbf{m}(\mathbf{x})$ is a smooth function of $\mathbf{x}$, then there exists some positive number ε_0 such that the perturbed map, $\mathbf{M}(\mathbf{x}) + \varepsilon\mathbf{m}(\mathbf{x})$, can be transformed to the original map $\mathbf{M}$ by a one to one change of variables for all ε satisfying $|\varepsilon| < \varepsilon_0$. (This change of variables is continuous but may not be differentiable.) In particular, in the range $|\varepsilon| < \varepsilon_0$, the perturbed map and the original map have the same number of periodic orbits for any period, and have the same symbolic dynamics.

An example of chaotic attractors that are apparently not structurally stable are those occurring for the logistic map $x_{n+1} = rx_n(1 - x_n)$. In this case, we saw in Section 2.2 that r-values yielding attracting periodic orbits are thought to be dense in r. Thus, for the case where r is such that there is a chaotic attractor, an arbitrarily small change of r (which can also be said to produce an arbitrarily small change in the map) can completely change the character of the attractor[3] (i.e., from chaotic to periodic).

As mentioned previously, the generalized baker's map and the horseshoe map yield examples of hyperbolic sets. For the generalized baker's map, Eq. (3.7), the Jacobian matrix is

$$\mathbf{DM}(\mathbf{x}) = \begin{bmatrix} \lambda_x(y) & 0 \\ 0 & \lambda_y(y) \end{bmatrix}, \tag{4.28}$$

where $\lambda_x(y) = \lambda_a$ or λ_b for $y < \alpha$ and $y > \alpha$, respectively, and $\lambda_y(y) = \alpha^{-1}$ or β^{-1} for $y < \alpha$ and $y > \alpha$, respectively. Since $\lambda_x(y) < 1$ and $\lambda_y(y) > 1$, the unstable manifolds are vertical lines and the stable manifolds are horizontal lines. Similar considerations apply for the horseshoe, where the stable and unstable manifolds are also horizontal and vertical lines. (In fact they are Cantor sets of horizontal and vertical lines whose intersection is the invariant set.) Another example is the Anosov map,

$$\begin{bmatrix} x_{n+1} \\ y_{n+1} \end{bmatrix} = \begin{bmatrix} 1 & 1 \\ 1 & 2 \end{bmatrix} \begin{bmatrix} x_n \\ y_n \end{bmatrix} \text{ modulo } 1. \tag{4.29}$$

Since x and y are taken modulo 1, they may be viewed as angle variables, and this map is a map acting on the two-dimensional surface of a torus.

The coordinates specifying points on this surface are the two angles x and y, one giving the location the long way around the torus, the other giving the location the short way around the torus, as shown in Figure 4.13(*a*). (Here one circuit around is signified by increasing the corresponding angle variable by one, rather than by 2π.) The map is continuous (i.e., two points near each other on the toroidal surface are mapped to two other points that are near each other) by virtue of the fact that the entries of the matrix are integers (note the modulo 1 in (4.29)). This map is hyperbolic and structurally stable. To see this, we note that, by virtue of the linearity of (4.29), the Jacobian matrix $\mathbf{DM}(\mathbf{x})$ is the same as the matrix in (4.29) specifying the map. The eigenvalues of the matrix (4.29) are $\lambda_1 = (3 + \sqrt{5})/2 > 1$ and $\lambda_2 = (3 - \sqrt{5})/2 < 1$. Thus, there are one-dimensional stable and unstable directions that are just the directions parallel to the eigenvectors of the matrix which are $(1, \lambda_{1,2} - 1)$.

For typical initial conditions the map (4.29) generates orbits which eventually come arbitrarily close to any point on the toroidal surface. Furthermore, the typical orbit visits equal areas with equal frequency and hence the natural invariant measure is uniform on the toroidal surface. Note that this map is area preserving,

$$\det\begin{bmatrix} 1 & 1 \\ 1 & 2 \end{bmatrix} = 1$$

The book by Arnold and Avez (1968) contains the illustration of the action of the map (4.29) which we reproduce in Figure 4.13(*b*). A picture

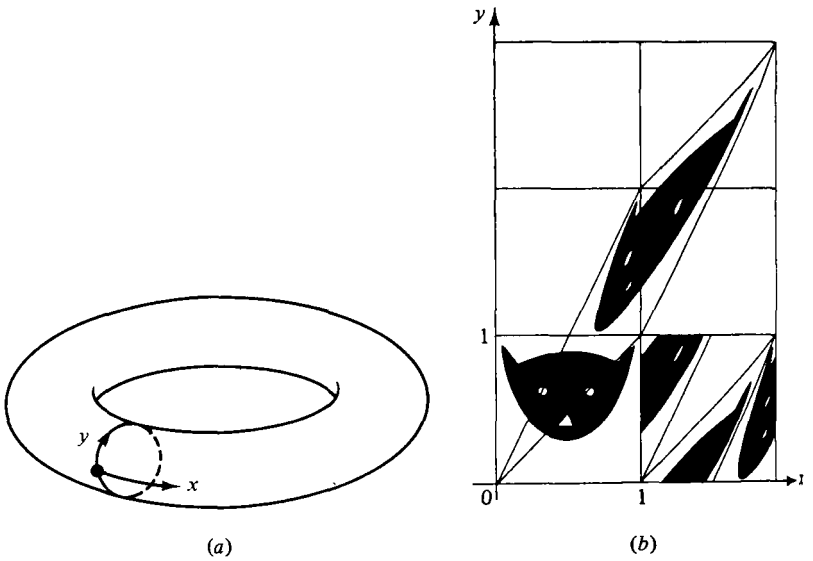

(*a*) (*b*)

Figure 4.13 The cat map. Note the mixing action of the map.

of the face of a cat is shown on the surface before the map is applied. Neglecting the modulo 1 operations, the square is mapped to a stretched out parallelogram which is returned to the square when the modulo 1 is taken. Because of this picture, (4.29) has been called the 'cat map.'

The map Eq. (3.17) considered by Sinai is a perturbation of Eq. (3.29) (the perturbation is the term $\Delta \cos(2\pi y_n)$). Thus, by the structural stability of (4.29), if Δ is not too large, the attractor for (3.17) is also hyperbolic and structurally stable (we do not know whether this is so for the value $\Delta = 0.1$ used for the plot in Figure 3.6).

While hyperbolic sets are very convenient mathematically, it is unfortunately the case that much of the chaotic phenomena seen in systems occurring in practice is nonhyperbolic and apparently not structurally stable. This seems to be the case for almost all practically interesting chaotic attractors examined to date. On the other hand, in cases of *nonattracting* chaotic sets, such as those arising in problems of chaotic scattering and fractal basin boundaries (see Chapter 5) hyperbolicity seems to be fairly common. As an example of a nonhyperbolic chaotic attractor we mention the Hénon attractor (Figure 1.12). The reason why the Hénon attractor fails to be hyperbolic is that there are points $\mathbf{x}$ on the attractor at which the stable and unstable manifolds $W^s(\mathbf{x})$ and $W^u(\mathbf{r})$ are tangent. We can regard the attractor itself as being the closure of the unstable manifold of points on the attractor.[4] Numerical calculations of stable manifolds of the attractor reveal the structure shown in Figure 4.14, which, according to the discussion in the caption, shows that there are tangencies of stable and unstable manifolds. We require for hyperbolicity that $E^s_{\mathbf{x}} \oplus E^u_{\mathbf{x}}$ span the tangent space at every point $\mathbf{x}$ on the attractor. Since the tangents to $W^s(\mathbf{x})$ and $W^u(\mathbf{x})$ coincide for $\mathbf{x}$ at such points, $E^s_{\mathbf{x}}$ and $E^u_{\mathbf{x}}$ cannot be defined at tangency points, and the Hénon attractor is thus not hyperbolic.

4.4 Lyapunov exponents

Lyapunov exponents give a means of characterizing the stretching and contracting characteristics of attractors and other invariant sets. First consider the case of a map $\mathbf{M}$. Let $\mathbf{x}_0$ be an initial condition and $\mathbf{x}_n$ ($n = 0, 1, 2, \ldots$) the corresponding orbit. If we consider an infinitesimal displacement from $\mathbf{x}_0$ in the direction of a tangent vector $\mathbf{y}_0$, then the evolution of the tangent vector, given by

$$\mathbf{y}_{n+1} = \mathbf{DM}(\mathbf{x}_n) \cdot \mathbf{y}_n, \tag{4.30}$$

determines the evolution of the infinitesimal displacement of the orbit from the unperturbed orbit $\mathbf{x}_n$. In particular, $\mathbf{y}_n/|\mathbf{y}_n|$ gives the direction of